Near-threshold study of the polarization of He resonance radiation using an energy-selected electron beam

C. Norén and J. W. McConkey
Department of Physics, University of Windsor, Windsor, Ontario, Canada N9B 3P4

P. Hammond
Department of Physics, University of Manchester, Manchester M13 9PL, United Kingdom

K. Bartschat
Department of Physics, Drake University, Des Moines, Iowa 50311-4505

(Received 4 October 1995)

The linear polarization of resonance vacuum-ultraviolet vuv radiation emitted from collisionally excited helium atoms has been measured in the threshold region below 25 eV. The apparatus consisted of a hemispherically analyzed electron beam interacting with a gas jet; the normally emitted radiation was analyzed using reflection optics. The threshold polarization was measured to be unity, in agreement with arguments based on the conservation of angular momentum. The measured vuv excitation functions and corresponding polarization curve were compared to 11-state R-matrix calculations of the excitation of the $2\,^1P$ state and excellent agreement was observed up to the $n=3$ threshold. Negative-ion resonances and cascade had pronounced effects on the observed sublevel excitation functions and on the polarization.

PACS number(s): 34.80.Dp, 42.25.Ja

I. INTRODUCTION

The importance of the polarization of optical radiation is being increasingly recognized in a variety of fields [1,2]. These include absolute calibration of spectroscopic equipment, plasma diagnostics, astrophysics, and electron-impact excitation studies. Whenever a population imbalance among magnetic sublevels of an excited state occurs, polarized fluorescence results. The imbalance can occur whenever the excitation processes are spatially anisotropic, such as occurs when polarized light beams or charged particle beams are used for the excitation process.

Clearly, when considering electron-impact excitation of atoms or molecules, the polarization of the resultant radiation carries important information about the process itself. This is likely to be particularly important near threshold, where conservation of the angular momentum and its components in the quantization (electron-beam) direction allows accurate predictions about the magnitude of the polarization in this energy region. Deviations from this expected value can be interpreted as being due to processes other than direct excitation. Although there have been numerous reports of near-threshold polarization of electron-impact radiation from a variety of targets, these have all been confined to the visible or near uv spectral regions (see the review by Heddle and Gallagher [3] which gives references to earlier work).

In an earlier publication [4] from this laboratory we presented data on the polarization of the vacuum-ultraviolet (vuv) resonance radiation from He and Ne targets over an energy range from threshold to 500 eV. These data were obtained with an unselected electron beam, so that the energy resolution was on the order of 1 eV. In the present paper we discuss data taken using an electron monochromator, so that a greatly improved energy resolution was obtained. This has allowed the near-threshold region to be studied in much greater detail than before. Preliminary reports on various aspects of this work have been presented elsewhere [5–9].

II. BASIC THEORY

The basic groundwork, relative to the polarization of atomic line radiation excited by electron impact, was laid in the classic paper of Percival and Seaton [10]. This paper exposed the limitations of earlier treatments, and provided formulas for the line polarization as a function of electron-impact energy in terms of magnetic sublevel cross sections and appropriate coefficients. The threshold selection rule $\Delta M_L=0$, which is based on conservation of angular momentum arguments, allows the threshold polarization to be obtained directly. The depolarizing effects of fine and hyperfine interactions were also dealt with by these authors. The situation is straightforward if the fine or hyperfine separations are either small or large compared to the natural linewidth.

Blum [11] gives the following expression for the threshold polarization P_T:

$$P_T=\frac{\left(\frac{15}{2}\right)^{1/2}(-1)^{L_2}G(L)_2\begin{Bmatrix}1&1&2\\L&L&L_2\end{Bmatrix}\begin{pmatrix}L&L&2\\0&0&0\end{pmatrix}}{\frac{1}{\gamma}\frac{2}{3(2L+1)}+\left(\frac{5}{6}\right)^{1/2}(-1)^{L_2}G(L)_2\begin{Bmatrix}1&1&2\\L&L&L_2\end{Bmatrix}\begin{pmatrix}L&L&2\\0&0&0\end{pmatrix}}, \tag{1}$$

where L and L_2 represent the orbital angular momentum of the upper and lower states of the observed decay, γ is the lifetime of the state in question, and $G(L)_2$ is a perturbation coefficient which takes account of the fine and/or hyperfine depolarizing effects. For the situation where both fine and hyperfine splittings are larger than the linewidth, and where the observation time is long compared to the lifetime, so that the time-dependent part of $G(L)_2$ drops out, we have

$$G(L)_2=\frac{1}{\gamma}\frac{1}{(2S+1)(2I+1)}\sum_{J,F}(2J+1)^2(2F+1)^2\begin{Bmatrix} J & F & I \\ F & J & 2 \end{Bmatrix}^2\begin{Bmatrix} L & J & S \\ J & L & 2 \end{Bmatrix}^2, \tag{2}$$

where the quantum numbers S, L, J, I, and F have the usual meanings and relationships.

Polarizations are difficult to measure in the near-threshold region not only because of low radiation intensities and the influence of cascade, but also because of the perturbing effect of negative-ion resonances in this energy region [12]. Comparison with the theoretically predicted threshold values in the past has often been limited to extrapolated experimental data.

If a $^1S\leftrightarrow{}^1P$ excitation decay is considered, (such as is the case for the resonance lines of He), then the polarization predicted using Eq. (1) is unity. A similar result is obtained by applying the threshold selection rule, $\Delta M_L=0$, as follows. If we assume that L and S are conserved separately, as is the case with helium, then the following relations for the magnetic sublevels must hold:

$$M_S+m_s=M_S'+m_s' \tag{3a}$$

$$M_L+m_l=M_L'+m_l', \tag{3b}$$

where M_L (M_L') is the orbital angular momentum magnetic quantum number before (after) electron impact, M_S (M_S') is the projection of the spin angular momentum before (after) electron impact, m_l (m_l') is the projection of the orbital angular momentum of the incident (scattered) electron onto the quantization axis, and m_s (m_s') is the projection of the spin of the incident (scattered) electron onto the quantization axis. For the case being considered, $M_S=M_S'=0$, and therefore Eq. (3a) becomes $m_s=m_s'$ always. If the incident electron defines the quantization axis, it has no angular momentum about this axis, and thus $m_l=0$. Also since the atom is initially in an $L=0$ state, $M_L=0$. At threshold the scattered electron carries off no energy and therefore no angular momentum (i.e., $m_l'=0$) which results in $M_L'=0$. Subsequent decay back to the ^1S ground state ($\Delta M_L=0$) will only produce radiation polarized parallel to the electron-beam direction. Since the polarization is defined as $(I_\parallel-I_\perp)/(I_\parallel+I_\perp)$ (see below), a threshold polarization of unity results.

If a temporary negative-ion resonance occurs close to threshold, then we note that coupling will occur between the two electrons involved, thus causing angular momenta to be transferred between the different components on the right-hand side of Eq. (3b). This causes the near-threshold arguments given above to be invalid, and hence we expect resonance features to show up as perturbations in the polarization curves.

Two further factors may influence the observed polarization in the near-threshold region. Cascade from more highly excited states is often less polarized, and thus can have a depolarizing effect on the transition under study. For example, in the case of He $n\ ^1P$ excitation, the cascade from ^1S states will be unpolarized. Second, as pointed out by Heideman, van de Water and Moergestel [13], electron correlation effects near the ionization threshold can have a significant effect on observed polarizations particularly when an atomic excitation involving a change in principal quantum number occurs. We note that such a change in principal quantum number is indeed the case for excitation of He($n\ ^1P$).

A suitable method to calculate the light polarizations in the near threshold region is the R-matrix (close-coupling) approach of the Belfast group. For the present case of interest, the 11-state model of Berrington *et al.* [14] should be sufficient, at least below the threshold of the $n=3$ states. For higher impact energies, this approach is not appropriate due to the importance of higher discrete and continuum target states in the close- coupling expansion. A better method for this energy region is the convergent close-coupling approach of Fursa and Bray [15]. However, this method would be computationally very expensive, since it does not take advantage of the R-matrix approach that allows for the fast calculation of many collision energies, once the problem has been solved for a single energy. On the other hand, the ability to calculate many energies efficiently is very important in the resonance region. Another possibility would therefore be the J-matrix method of Konovalov and McCarthy [16]. In any case, all theoretical results would need to be corrected for cascades at energies above the $n=3$ thresholds. This is a nontrivial problem, and will not be discussed in this paper.

Figures 1 and 2 provide an impression about the detailed resonance structure near the $2\ ^1P$ threshold, both for the sublevel-resolved total excitation cross sections (Fig. 1) and for the corresponding polarization function (Fig. 2). As would be expected in the 11-state approach, the value of the light polarization converges to $+1$ at threshold, and becomes a smooth function for energies above the highest $n=3$ level.

III. EXPERIMENT

A schematic of the apparatus is shown in Fig. 3. Electrons from a thoriated tungsten filament source were energy selected using a hemispherical analyzer, and focused through a target gas beam into a Faraday cup. Currents were typically 20 nA, with an energy spread of approximately 160 meV. Improvements in this energy resolution were possible, but only at the expense of significant reductions in the beam current. Because we were interested in the near-threshold region of the excitation functions, where signal intensities are low, we had to adopt this compromise of current and resolution. The vacuum chamber was lined with a layer of conetic shielding to minimize the effect of stray magnetic fields. Improved performance of the electron monochromator in terms of achievable current and long-term stability was achieved by keeping the whole system warm using a quartz iodine projection lamp heater inside the vacuum tank. The

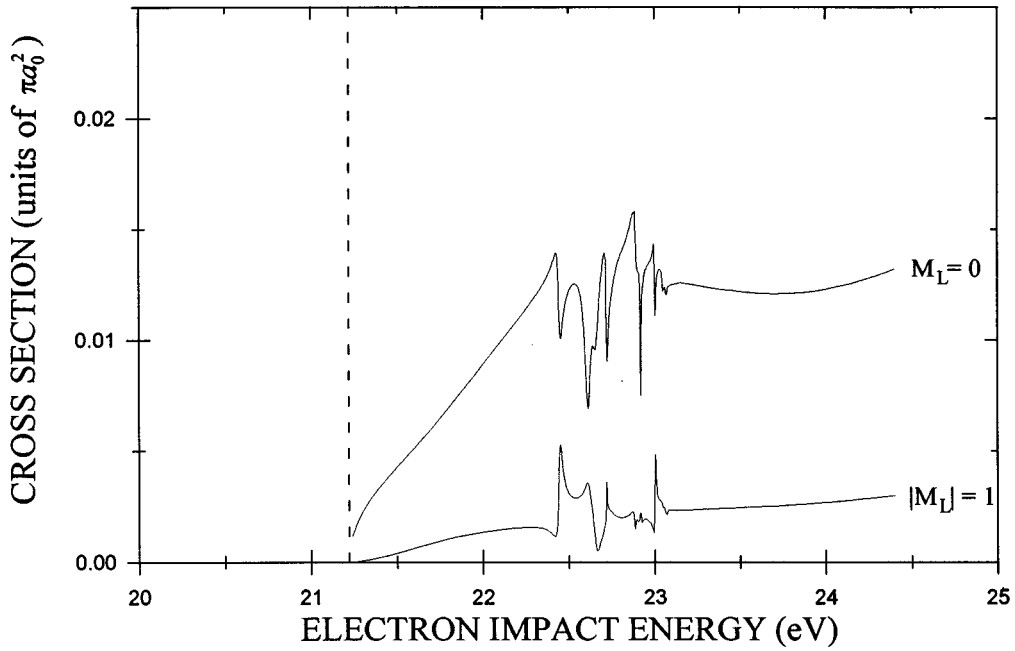

FIG. 1. 11-state R-matrix calculations for the excitation of the $2\,^1P$ state of helium as a function of electron impact energy. The excitation functions for $M_L=0$ and $|M_L|=1$ are shown in the diagram. The vertical line indicates the $2\,^1P$ threshold (21.22 eV).

metastable atom detector, situated directly beneath the gas beam, consisted of a channel electron multiplier (Galileo 4039-C). This provided a convenient means of energy calibration and system tuning. Observation of the prominent negative ion resonances, which occur near threshold [17,18], allowed an estimate of both the electron-impact energy and the energy resolution to be readily obtained. Normally metastable excitation functions were obtained immediately before and after a polarization measurement. These enabled the energy scale to be established, and possible drifts in energy by the system to be monitored.

Radiation from the interaction region, emitted orthogonal to the electron beam, traversed a single-reflection polarization analyzer, 10 cm from the interaction region, and was detected using a channel electron multiplier (Galileo 4039-C). The optical element in the analyzer was a 1-m-diameter, optically flat, gold-coated Pyrex mirror (Janos Optical Corp.) mounted so that the angle of incidence was 57.5°. The orientation of the analyzer was set using a stepper motor under computer control. Thus complete polarization ellipses could be plotted or, more usually, data could be collected at four orthogonal positions of the analyzer corresponding to detection of $I_{\parallel}^{m}$ or $I_{\perp}^{m}$, where these parameters refer to measured intensities with the analyzer set to transmit light preferentially polarized parallel and perpendicular, respectively, to the electron-beam (quantization) axis. Data from the detector

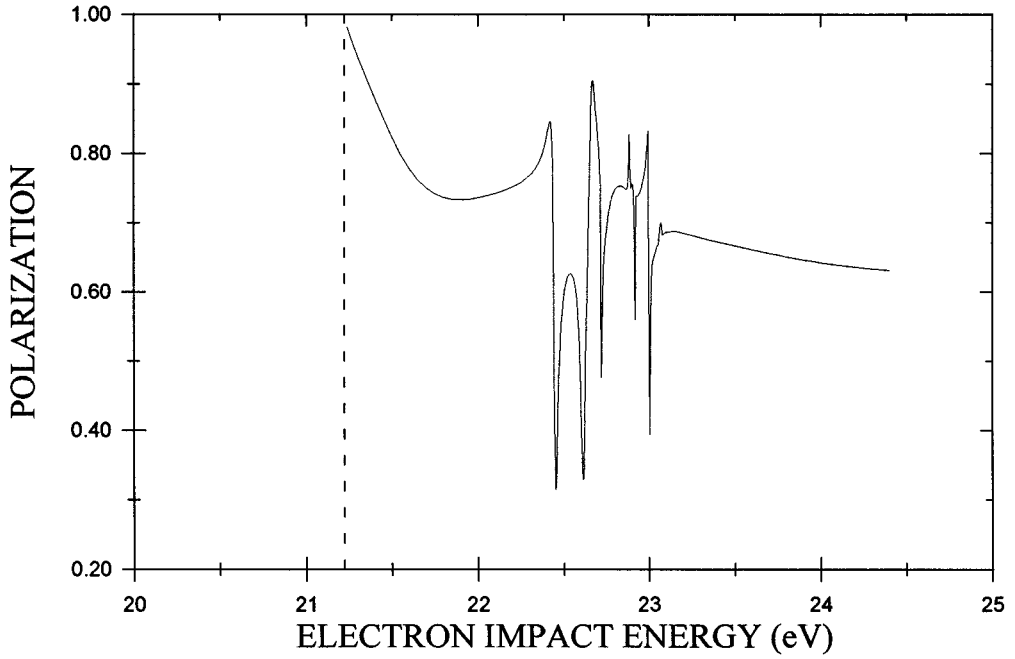

FIG. 2. 11-state R-matrix calculation of the polarization function for the $2\,^1P-1\,^1S$ radiation as a function of electron impact energy. The vertical line indicates the $2\,^1P$ threshold (21.22 eV).

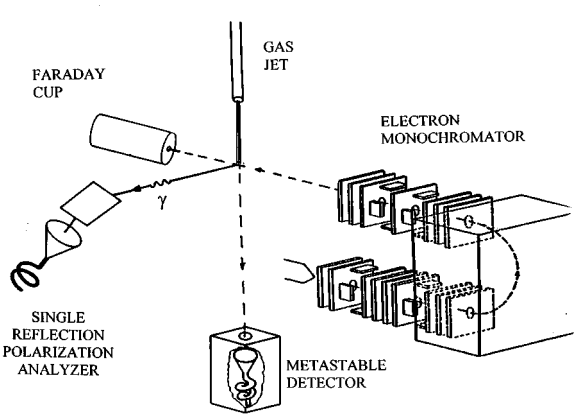

FIG. 3. Schematic diagram of the experimental setup.

were routed into the memories of a multichannel analyzer. Automatic scanning of electron-beam energy could be carried out so that the variation of $I_{\parallel}^{m}$ and $I_{\perp}^{m}$, and hence polarization P, as function of impact energy could be obtained directly. Any slight residual misalignment of the analyzer was taken into account by averaging the two $I_{\parallel}^{m}$ and $I_{\perp}^{m}$ count rates.

The polarization P of the radiation is defined in the usual way as $(I_{\parallel}-I_{\perp})/(I_{\parallel}+I_{\perp})$, where $I_{\parallel}$ and $I_{\perp}$ are the true intensities. For a single reflection the measured intensities $(I_{\parallel}^{m},I_{\perp}^{m})$ are related to the true values $(I_{\parallel},I_{\perp})$ by

$$\begin{aligned} I_{\parallel}^{m}&=D(R_{\parallel}I_{\parallel}+R_{\perp}I_{\perp}),\\ I_{\perp}^{m}&=D(R_{\perp}I_{\parallel}+R_{\parallel}I_{\perp}), \end{aligned} \tag{4}$$

where D is the channeltron detection efficiency, and $R_{\parallel}$ and $R_{\perp}$ are the reflection coefficients for photons whose electric vector lies parallel and perpendicular, respectively, to the plane of incidence. The axis of the channeltron was mechanically aligned along the optic axis to ensure its polarization insensitivity.

Using Eq. (4) yields the following expression for the polarization:

$$P=\frac{(R_{\parallel}+R_{\perp})}{(R_{\parallel}-R_{\perp})}\frac{(I_{\parallel}^{m}-I_{\perp}^{m})}{(I_{\parallel}^{m}+I_{\perp}^{m})}=\frac{1}{\eta}\frac{(I_{\parallel}^{m}-I_{\perp}^{m})}{(I_{\parallel}^{m}+I_{\perp}^{m})}, \tag{5}$$

where η is the polarization efficiency.

By inverting Eq. (4), relations for the true intensities can be obtained:

$$\begin{aligned} I_{\perp}&=\frac{(\tau I_{\perp}^{m}-I_{\parallel}^{m})}{DR_{\perp}(\tau^{2}-1)},\\ I_{\parallel}&=\frac{(\tau I_{\parallel}^{m}-I_{\perp}^{m})}{DR_{\perp}(\tau^{2}-1)}, \end{aligned} \tag{6}$$

where

$$\tau=\frac{R_{\parallel}}{R_{\perp}}=\left(\frac{1+\eta}{1-\eta}\right). \tag{7}$$

To obtain the efficiency (η) of the polarizer, we normalized our polarization data using the earlier measurements of Hammond *et al.* [4] and Karras [19]. They used multiple mirror polarizers to make the measurements insensitive to the mirror efficiency. The normalization was carried out at an energy well away from threshold in a region which was unperturbed by resonance effects and where the polarization was a relatively slowly varying function with impact energy.

Studies of the variation of P with gas pressure were carried out to ensure freedom from depolarizing effects such as imprisonment of resonance radiation. This meant that the background pressure in the system did not exceed 2×10^{-6} torr when the gas beam was operational. Background effects due, for example, to small contributions to the measured signals from the background gas in the system, were accounted for as discussed by Hammond *et al.* [4]. The base pressure without the target gas being introduced was 2×10^{-7} torr.

IV. ERRORS

The total estimated errors of the data are designated by error bars in each of the figures. The total error includes (i) the statistical uncertainties in the raw data collection which were less than 1% except in the near-threshold region, (ii) the uncertainty in the background subtraction which involved extrapolation of background counts from below the vuv threshold, and (iii) the determination of η (and thus τ) by calibrating to the data of Hammond *et al.* [4]. Other systematic errors such as those caused by mechanical misalignment are minimized by the averaging technique described above.

As noted by Hammond *et al.* [4], caution must be used when interpreting the data since the analyzer and detector have different efficiencies over the spectral range of the He vuv photons (50.5–58.4 nm). Below 23.09 eV only the 58.4-nm line is present, which simplifies analysis. However, above this energy, vuv radiation from $n\ ^{1}P$ states ($n\geqslant3$) becomes present as their excitation energy is reached, and therefore each line would have to be analyzed with the appropriate coefficients for its wavelength. This is not possible in the present setup, and so the coefficients based on the 58.4-nm radiation were used since it is the dominant line. The quoted errors do not take into account this situation.

V. RESULTS AND DISCUSSION

The measurement of the integrated vuv photons $(n\ ^{1}P\rightarrow1\ ^{1}S)$ as a function of electron impact energy is presented in Fig. 4. The data have been corrected for the polarization sensitivity of the analyzer using Eqs. (6) and (7) (D and $R_{\perp}$ were set equal to 1 since they divide out in polarization calculations). A linear background (which is an extrapolation of background noise counts below threshold to higher electron energies) has been subtracted from the data, but no correction for variations with energy of the electron-beam current has been performed. The data have been normalized to the 11-state R-matrix calculations with the same normalization factor being used for both the parallel and perpendicular data. The energy scale was calibrated by adding together $I_{\parallel}$ and $I_{\perp}$ and comparing the location of the feature at 22.67 eV with the vuv data of Brunt, King, and Read [20]. The polarization curve resulting from the vuv data shown in Fig. 4 is presented in Fig. 5. All data points below the threshold have been suppressed since this value lies within the

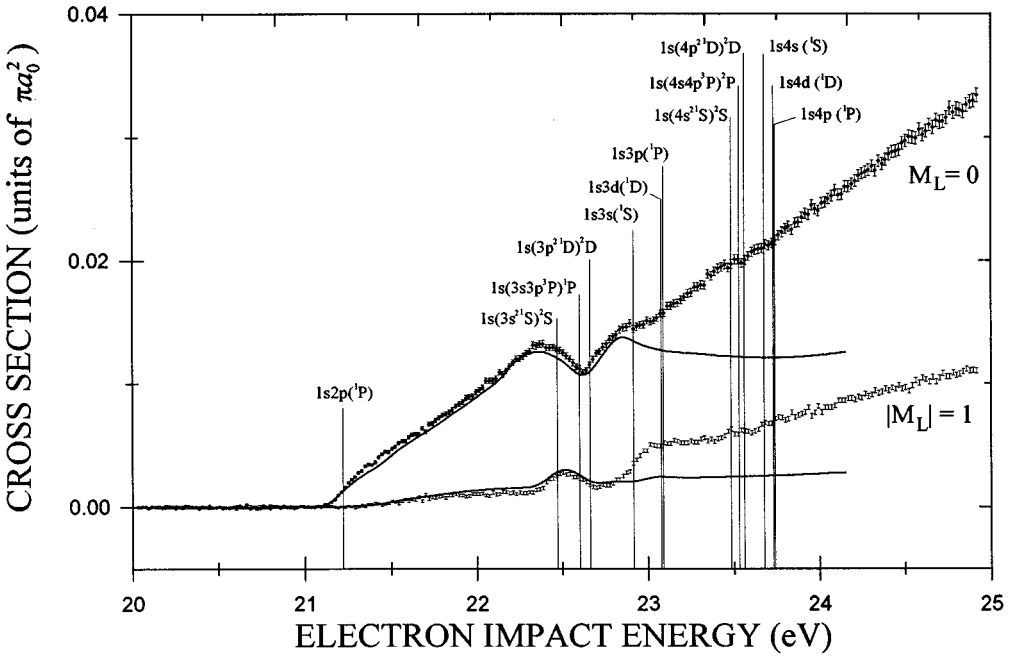

FIG. 4. vuv excitation functions for helium ($n\ ^1P-1\ ^1S$) radiation as a function of electron impact energy. The data has been corrected for the polarization sensitivity of the analyzer. Upper, $M_L=0$, and lower, $|M_L|=1$, curves refer to $I_\parallel$ and $I_\perp$, respectively (see text). The solid line represents the 11-state R-matrix calculations for $2\ ^1P-1\ ^1S$ radiation convoluted with a 160-meV Gaussian function. The vertical lines on the diagram indicate the positions of relevant neutral and negative-ion states. Error limits are shown, and are discussed in the text.

large error bars ($>\pm 1$) of these data. The determination of η was done by comparing the polarization values calculated using $I_\parallel^m$ and $I_\perp^m$ measured at 24 eV (using the above data) and at 30 eV (from a separate measurement) with values obtained by Hammond *et al.* [4]. A value of $1/\eta=1.95$ was obtained at both energies. Also shown in Figs. 4 and 5 are the 11-state R-matrix calculations which have been convoluted by a Gaussian function with a full width at half maximum (FWHM) of 160 meV. It can be seen immediately that there is excellent agreement between the experimental and theoretical data sets.

The positions of some of the neutral and negative-ion states are indicated on the figures. In the first eV above threshold (21.22 eV) there are no perturbing resonances present, and thus the polarization function is entirely due to the $2\ ^1P-1\ ^1S$ transition (58.4 nm). The polarization function is observed to slowly drop in value over this range and this lack of structure near the threshold is in contrast to what is observed in the visible transitions of helium [21,22] and in the vuv transitions of the heavy rare gases [23]. Theory also predicts this slow variation in value, but underestimates slightly the absolute values above 21.5 eV. This situation presents not only an excellent opportunity to test the threshold angular momentum arguments presented in Sec. II, but also allows one to see how the polarization of pure direct excitation varies with impact energy.

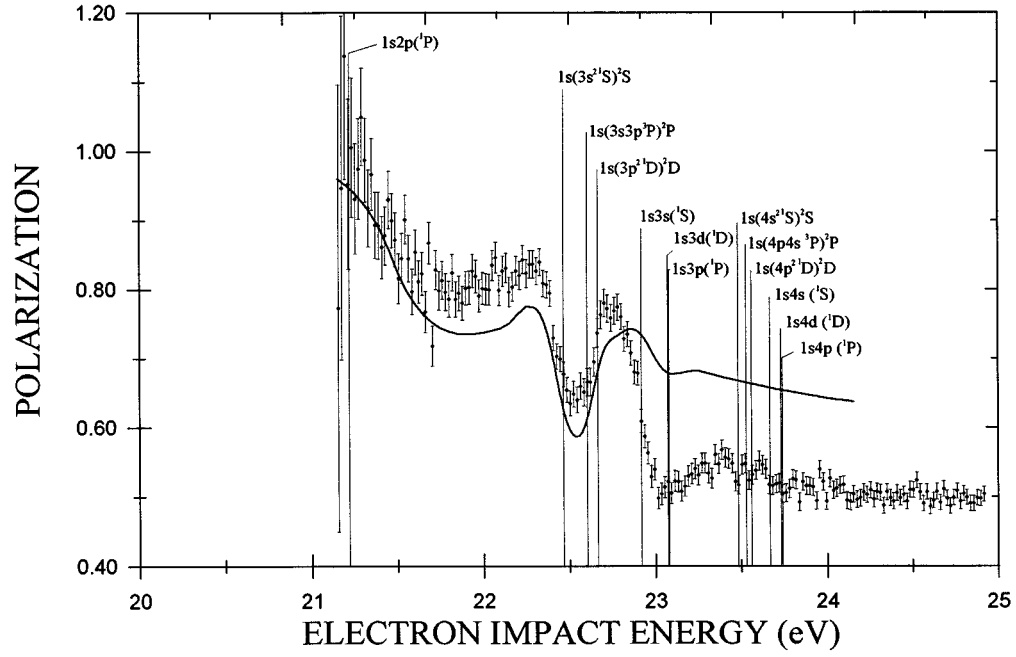

FIG. 5. Polarization function for helium ($n\ ^1P-1\ ^1S$) radiation as a function of electron impact energy. The solid line represents the 11-state R-matrix calculation for the $2\ ^1P-1\ ^1S$ radiation convoluted with a 160-meV Gaussian function. The vertical lines on the diagram indicate the positions of relevant neutral and negative-ion states. Error limits are shown, and are discussed in the text.

The threshold polarization is predicted to be +1 from simple angular momentum arguments (see Sec. II), and from Fig. 5 it is clearly seen that the polarization function goes to unity. This effect can be seen clearly also in the $I_{\parallel}$ and $I_{\perp}$ near-threshold excitation functions (Fig. 6), where the signal in the parallel channel sharply increases at threshold (allowing for the energy resolution) while the signal in the perpendicular channel remains essentially at zero for a further 0.15 eV. Using this result we can make predictions concerning the nature of the scattering process just above threshold.

We consider the following excitation schemes:

$$e^-(ks)+\mathrm{He}(1s^2\ ^1S)\rightarrow e^-(kp)+\mathrm{He}^*(1s2p\ ^1P), \quad (8a)$$

$$e^-(kp)+\mathrm{He}(1s^2\ ^1S)\rightarrow e^-(ks)+\mathrm{He}^*(1s2p\ ^1P). \quad (8b)$$

Other excitation paths are not considered because they would require incident and/or scattered electrons with higher angular momentum. Above threshold, both paths are allowed by parity and angular momentum conservation laws. However path (8b) has the additional requirement that only magnetic sublevels with a quantum number equal to 0 are possible for the atomic state. This is because an s electron is scattered (the sum of the orbital angular momentum z components must equal 0) while for path (8a) atomic sublevels with quantum numbers equal to 0 and ± 1 are allowed since a p-wave electron is scattered. Since the measured perpendicular intensity ($|\Delta M_L|=1$) in the resultant decay is zero above threshold, this suggests that path (8b) is responsible for the scattering process. Thus s-wave scattering is the dominant process in the near-threshold region. Assuming this is the case, excitation of $2\ ^1P$ close to threshold could have significant possibilities in the area of calibration of the behaviour of electron spectrometers used with very low-energy electrons [24].

In other He polarization experiments [21,22], the polarization was observed to change rapidly within the first 100 meV above threshold, suggesting that higher angular momentum electrons were being scattered. However, the above comments coupled with the resonance calculations and measurements by Wolcke *et al.* [25] for mercury as well as heavy rare gas measurements [23,26] indicate that negative-ion resonances are most likely responsible for these rapid changes.

The effect of the resonances first appear at approximately 22.4 eV, where strong broad features are evident. The polarization function appears to level out at a value of 0.8, before coming under the influence of the $1s(3s^2\ ^1S)^2S$, $1s(3s3p\ ^3P)^2P$, and $1s(3p^2\ ^1D)^2D$ resonances that have been observed [27] between 22.47 and 22.66 eV. From the convoluted theoretical data it can be seen that these resonances are responsible for the oscillating shape of the polarization function in this region.

The effects of the resonances and cascade can be seen clearly in the excitation functions, Fig. 4. Referring to this figure, it can be seen that the resonances affect the $I_{\parallel}$ and $I_{\perp}$ excitation functions differently. This highlights the care which must be exercised when making comparisons between optical excitation function measurements (where usually $I_{\parallel}+I_{\perp}$ is observed) and the total excitation function measurements which correspond to $I_{\parallel}+2I_{\perp}$. Thus resonance features could actually appear at different energies in the two types of curves.

The theoretical predictions for the excitation of the $2\ ^1P$ state show excellent agreement with the observed excitation functions for energies up until just below the threshold of the first cascading state ($3\ ^1S$). Above the threshold for $3\ ^1S$, increases in the signal for both the parallel and perpendicular channels are observed, as would be expected. To see the effects of the cascading states and higher-lying $n\ ^1P$ ($n\geqslant 3$) states more clearly, the theoretical excitation curves were subtracted from the corresponding measured excitation curves, and the results are presented in Fig. 7. Just below the onset of the $3\ ^1S$ state, the excitation functions for the paral-

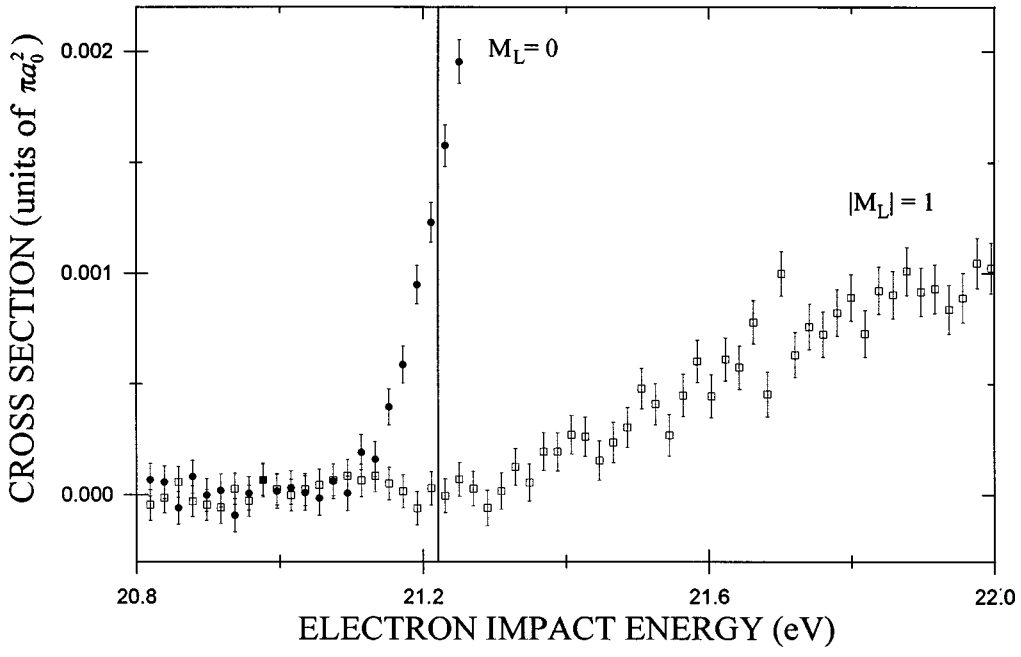

FIG. 6. Near-threshold vuv excitation functions for helium ($2\ ^1P-1\ ^1S$) transitions as a function of electron impact energy. The data have been corrected for the polarization sensitivity of the analyzer. The vertical line represents the nominal threshold for the $2\ ^1P$ state.

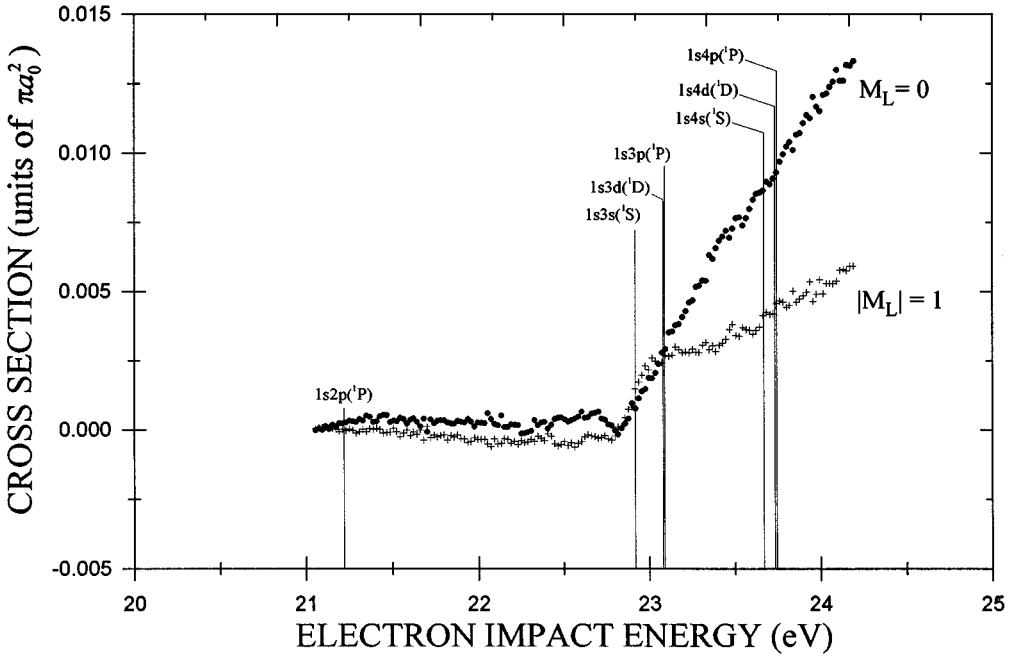

FIG. 7. Cascade contribution to $2\,^1P$ excitation obtained as discussed in the text. The vertical lines on the diagram indicate the positions of relevant neutral states.

lel and perpendicular channels are shown to rise quickly and identically. This confirms that the cascade from this state is unpolarized, as noted above. We also note that at the thresholds of the $3\,^1D$ and $3\,^1P$ states, the contribution to the parallel channel clearly dominates over the perpendicular channel. This is not unexpected since, in the absence of any perturbing negative-ion resonances, the excitation function for the $3\,^1P$ state should be similar to that of $2\,^1P$ in the threshold region and thus favor the parallel channel (see Fig. 6). The $3\,^1D$ state will decay to the $2\,^1P$ state, and, from the analysis of Percival and Seaton [10], this unobserved radiation will have a threshold polarization of 0.6 (recall from Sec. II that only $M_L=0$ is excited). This would result in 80% of the $3\,^1D$ state decaying to the $M_L=0$ sublevel of $2\,^1P$, and therefore the parallel channel would be enhanced. We note that the measurements of Heddle, Keesing, and Parkin [22] on the polarization of $3\,^1D-2\,^1P$ radiation indicate large positive values ($\geqslant 0.4$) close to threshold. Above threshold, the $M_L=\pm 1$ and $M_L=\pm 2$ sublevels of $3\,^1D$ can be populated, which complicates the analysis. Note that $M_L=\pm 2$ sublevels of $3\,^1D$ can only decay to the $M_L=\pm 1$ sublevels of $2\,^1P$.

Total cross sections (i.e., $Q_{M_L=0}+2Q_{|M_L|=1}$) for the excitation of the cascading and the $n\,^1P$ ($n\geqslant 3$) states have been obtained using the data in Fig. 7, and the magnitude of the observed values in the near-threshold region are consistent with theoretical calculations of Konovalov and McCarthy [16] for the excitation of $3\,^1S$, $3\,^1D$, and $3\,^1P$.

After the $(3p^2\,^1D)^2D$ resonance one would expect the polarization function (Fig. 5) to return to the background level which would lie near 0.7 based on (i) an extrapolation to lower energies of the cascade-free values measured by Steph and Golden [28], and (ii) the theoretical R-matrix calculations discussed earlier. However the observed polarization falls dramatically to $\sim$0.5. This can be attributed to the excitation of the $3\,^1S$ state which cascades to the $2\,^1P$ state. This causes a net depolarization in the radiation being emitted from the $2\,^1P$ state. When the $3\,^1D$ and $3\,^1P$ thresholds are reached, an enhancement of the $M_L=0$ population occurs, as discussed above, leading to a positive enhancement of the polarization, as is observed above 23 eV.

The small perturbations in the polarization curve (Fig. 5) at the opening of the $n=4$ excitation channel, near 23.5 eV, can also be seen in the excitation function curves of Fig. 4. The explanation, in terms of resonance excitation and cascade, is most probably very similar to that discussed in connection with the structures around the $n=3$ thresholds. Heddle, Keesing, and Parkin [22] have studied the $4\,^1S$ and $4\,^1D$ excitation functions and have observed similar behavior to those with $n=3$. The statistical scatter of the data near the ionization threshold (24.59 eV) prevents any definitive conclusion on correlation effects, such as discussed by Heideman, van de Water, and Moergestel [13], other than that, if present, they are small.

In summary the shape of the polarization curve (Fig. 5) can be understood as follows.

(1) The threshold is governed by angular momentum conservation and is dominated by s-wave scattering.

(2) Above threshold the polarization falls from unity due to scattered electrons being able to possess higher l partial waves.

(3) $nlnl'$ families of resonances cause perturbations in the polarization around 22.6 ($n=3$) and 23.6 eV ($n=4$).

(4) Cascading from $n=3$ and 4 neutral states at approximately 23 and 23.8 eV, respectively, causes the polarization to decrease from that due to pure direct excitation.

VI. CONCLUSIONS

The polarization function for the integrated vuv radiation resulting from electron impact on He atoms has been measured in the threshold region. At threshold the polarization

function was observed to go to unity in agreement with angular momentum conservation laws. Analysis of the vuv photon excitation functions at threshold indicates that s-wave scattering is dominant in this region. Above the threshold region the data clearly display perturbations due to negative-ion resonance formation and the depolarizing effects of cascade from higher-lying neutral states. The data obtained from 11-state R-matrix calculations for the $2\,^1P$ state were in excellent agreement with the observed curves. Electron correlation effects at the ionization threshold were not significant.

ACKNOWLEDGMENTS

The authors are pleased to acknowledge financial assistance from the Natural Sciences and Engineering Research Council of Canada, and expert technical help from the staff of the mechanical and electronic shops at Windsor. P.H. acknowledges the financial support of the UK Engineering and Physical Sciences Research Council. K.B. acknowledges financial support from the United States National Science Foundation under Grant No. PHY-9318377.

[1] T. Fujimoto, F. Koike, K. Sakimoto, R. Okasaki, K. Kawasaki, K. Takiyama, T. Oda, and T. Kato, National Institute for Fusion Science Report No. NIFS-DATA-16, Nagoya, Japan, 1992 (unpublished).

[2] S. A. Kazantsev and J.-C. Hénoux, *Polarization Spectroscopy of Ionized Gases* (Kluwer, Boston, 1995).

[3] D. W. O. Heddle and J. W. Gallagher, Rev. Mod. Phys. **61**, 221 (1989).

[4] P. Hammond, W. Karras, A. G. McConkey, and J. W. McConkey, Phys. Rev. A **40**, 1804 (1989).

[5] C. Norén and J. W. McConkey, Bull. Am. Phys. Soc. **35**, 1172 (1990).

[6] J. J. Corr, C. Norén, P. J. M. van der Burgt, and J. W. McConkey, in *Abstracts of the Seventeenth International Conference on the Physics of Electronic and Atomic Collisions, Brisbane, 1991*, edited by E. McCarthy, W. R. MacGillivary, and M. C. Standage (ICPEAC, Brisbane, 1991), p. 125.

[7] C. Norén and J. W. McConkey, Phys. Can. **48**, 99 (1992).

[8] C. Norén and J. W. McConkey, in *Abstracts of the Fourteenth International Conference on Atomic Physics, Boulder, 1994*, edited by C. E. Wieman and D. J. Wineland (ICAP, Boulder, 1994).

[9] C. Norén and J. W. McConkey, in *Abstracts of the Nineteenth International Conference on the Physics of Electronic and Atomic Collisions, Whistler, 1995*, edited by J. B. A. Mitchell, J. W. McConkey, and C. E. Brion (ICPEAC, Whistler, 1995), p. 461.

[10] I. C. Percival and M. J. Seaton, Philos. Trans. R. Soc. London Ser. A **251**, 113 (1958).

[11] K. Blum, *Density Matrix Theory and Applications* (Plenum, New York, 1981).

[12] D. W. O. Heddle, Contemp. Phys. **17**, 443 (1976).

[13] H. G. M. Heideman, W. van de Water, and L. J. M. Moergestel, J. Phys. B **13**, 2801 (1980).

[14] K. A. Berrington, P. G. Burke, L. C. G. Freitas, and A. E. Kingston, J. Phys. B **18**, 4135 (1985).

[15] D. Fursa and I. Bray, Phys. Rev. A **52**, 1279 (1995).

[16] D. A. Konovalov and I. E. McCarthy, J. Phys. B **28**, L139 (1995).

[17] J. N. H. Brunt, G. C. King, and F. H. Read, J. Phys. B **10**, 433 (1977).

[18] S. J. Buckman, P. Hammond, G. C. King, and F. H. Read, J. Phys. B **16**, 4039 (1983).

[19] W. Karras, M.Sc. thesis, University of Windsor, 1988 (unpublished).

[20] J. N. H. Brunt, G. C. King, and F. H. Read, J. Electron Spectrosc. Relat. Phenom. **12**, 221 (1977).

[21] D. W. O. Heddle, R. G. W. Keesing, and R. D. Watkins, Proc. R. Soc. London Ser. A **337**, 443 (1974).

[22] D. W. O. Heddle, R. G. W. Keesing, and A. Parkin, Proc. R. Soc. London Ser. A **352**, 419 (1977).

[23] C. Norén, Ph.D. thesis, University of Windsor, 1995 (unpublished).

[24] S. Trajmar and J. W. McConkey, Adv. At. Mol. Opt. Phys. **33**, 63 (1994).

[25] A. Wolcke, K. Bartschat, K. Blum, H. Borgmann, G. F. Hanne, and J. Kessler, J. Phys. B **16**, 639 (1983).

[26] J. E. Furst, M. K. P. Wijayaratna, D. H. Madison, and T. J. Gay, Phys. Rev. A **47**, 3775 (1993).

[27] S. J. Buckman and C. W. Clark, Rev. Mod. Phys. **66**, 539 (1994).

[28] N. C. Steph and D. E. Golden, Phys. Rev. A **26**, 148 (1982).